European Journal of Organic Chemistry

EurJOC
European Journal of Organic Chemistry

Chemistry Europe
European Chemical Societies Publishing

RESEARCH ARTICLE OPEN ACCESS

Chlorinated Paracyclophanes: Composition Analysis and Direct Metal-Free Alkylation with *n*-BuLi

Davide Frigatti[1] | Alessandro Scarso[1] | Stefan Bräse[2,3] | Fabrizio Fabris[1]

[1]Dipartimento di Scienze Molecolari e Nanosistemi, Università Ca' Foscari Venezia, Mestre Venezia, Italy | [2]Institut für Organische Chemie (IOC), Karlsruher Institut für Technologie (KIT), Karlsruhe, Germany | [3]Institut für Biological and Chemical Systems (IBCS-FMS), Karlsruher Institut für Technologie (KIT), Eggenstein-Leopoldshafen, Germany

Correspondence: Stefan Bräse (stefan.braese@kit.edu) | Fabrizio Fabris (fabrisfa@unive.it)

Received: 9 December 2025 | **Revised:** 14 January 2026 | **Accepted:** 16 January 2026

Keywords: aromatic alkylation | butyllithium | dibutyl[2.2]paracyclophane | dichloro[2.2]paracyclophane

ABSTRACT

A transition-metal-free alkylation of the dichloro[2.2]paracyclophane scaffold is reported, representing a significant advancement in the reactivity of this unique class of compounds. The pseudo-*para* isomer of dichloro[2.2]paracyclophane was isolated from a commercial mixture *via* crystallization, and its structure was assessed by detailed 1D and 2D NMR spectroscopy. The reaction of the purified isomer with butyllithium was investigated, and a systematic optimization revealed that reaction rate and selectivity were significantly improved by using a chelating agent and conducting the reaction in refluxing heptane. This refined protocol yielded the desired dialkylated product, establishing a new and more efficient synthetic pathway that opens the door to further exploration of this unprecedented reactivity.

1 | Introduction

[2.2]Paracyclophanes (PCPs) are unique molecular scaffolds characterized by two benzene rings linked by two ethylene bridges, resulting in a distinctive, strained, and rigid nonplanar aromatic system [1]. This inherent structural feature, which leads to through-space π–π electronic interactions and tunable configurational behaviors, has attracted significant interest across diverse fields [2], including molecular junctions [3], asymmetric catalysis [4–14], optical materials [15–22], and advanced materials science [23–29]. The ability to precisely modify the paracyclophane core through chemical functionalization is crucial for tailoring its steric, electronic [30], and optoelectronic [23–28] properties, thereby expanding its applications.

Poly(*p*-xylylene)s (Parylene or PPXs) are a class of polymers of technological interest, primarily utilized as conformal coating materials in diverse applications such as electronic devices [31], medical implants [32], stents [33], and pacemakers [33, 34]. Based on specialized market analysis, the global parylene market was valued at USD 1.38 billion in 2024 and is projected to reach USD 4.8 billion by 2031, driven by a Compound Annual Growth Rate (CAGR) of 3.13%. This growth reflects the increasing demand for high-performance polymer coatings in advanced technology sectors [35]. The unique synthesis of PPXs involves the vaporization and subsequent pyrolysis of PCP precursors, followed by chemical vapor deposition (CVD) and polymerization of the reactive quinodimethane intermediates under ambient conditions [36]. This distinctive process yields highly conformal, pinhole-free coatings on virtually any solid substrate, making them ideal as protective layers [37].

The physical and mechanical properties of PPXs, including their thermal behavior and flexibility, are significantly influenced by the substitution pattern of the parent PCP precursors [38]. Despite the promising characteristics of PPXs, the repertoire of their CVD-based derivatives with varied functionalities remains limited. Halogenated derivatives, such as poly(chloro-*p*-xylylene)

Dedicated to Prof. Armin de Meijere (1939–2025).

and poly(bromo-*p*-xylylene), are known to be partially crystalline and fusible, with the dichloro-substituted PPXs, demonstrating a notable increase in elongation at break, reaching 200% [39].

Only a limited number of PPXs featuring alkyl or phenyl substituents have been reported to date [40–45]. Methyl- and ethyl-substituted PPXs, synthesized *via* CVD from their respective PCP precursor, typically exhibit poor solubility. However, the introduction of *n*-alkyl chains at the aromatic ring has been shown to yield soluble PPXs. Specifically, a propyl group has been identified as the minimum chain length required to achieve solubility under ambient conditions [46].

It is generally expected that increasing the alkyl chain length in PPXs will enhance their coating flexibility while concurrently decreasing the glass transition temperature, leading to a reduction in crystallinity. This is supported by experimental findings showing that increasing the length of the alkyl chain decreased the glass transition temperature, decomposition temperature, and Young's modulus [46]. Furthermore, the elongation at break, with a best reported value of 380%, was improved in comparison to commercial PPXs [47].

Electrophilic aromatic substitution has been widely employed to introduce a diverse range of functional groups onto the PCP core, including bromo, nitro, and formyl groups, as well as amino, hydroxyl, thiol, trifluoromethanesulfonate, azido, diphenylphosphino, acetoxy, carboxyl, boronic acid, and trialkylstannyl functionalities [47]. Alkylation of aromatic systems is a fundamental transformation in organic synthesis, providing access to a wide array of functionalized molecules. Despite significant advancements in PCP chemistry, a persistent challenge remains in developing atom-economical and environmentally benign methods for the direct functionalization of PCPs. Specifically, the alkylation of PCP, particularly at the strained aromatic positions, typically relies on transition-metal-catalyzed coupling reactions. These methods, while powerful, can suffer from issues such as the presence of noxious catalyst residues, ligand requirements, and sensitivity to moisture or oxygen, which can complicate purification and limit their application in certain sensitive materials.

Herein, we report the unprecedented transition-metal-free alkylation of dichloro [2.2]paracyclophane (Cl_2-PCP). To achieve this goal, a preliminary isolation and characterization procedure for the Cl_2-PCP isomers was developed. For the pseudo-*para* isomer, we performed direct alkylation of the paracyclophane core without the need for a transition-metal catalyst, offering a significant advancement in the synthetic accessibility of functionalized paracyclophane derivatives. This novel approach overcomes the limitations associated with traditional metal-catalyzed processes, providing a more sustainable and efficient pathway for the introduction of alkyl groups onto this unique molecular scaffold. A plausible mechanism is proposed.

2 | Results and Discussion

2.1 | Isomer Separation of Galaxyl C

Galaxyl C is a commercial product containing a mixture of isomers of Cl_2-PCP whose structures are reported in Figure 1. Four stereoisomers are possible in which one chlorine atom is present on each aromatic ring. To facilitate the identification of products in the alkylation reactions and to ensure comprehension of the possible mechanism of the reaction, it was necessary to treat Galaxy C to isolate one of its isomers. Obtaining a starting material composed of a pure single isomer is crucial for achieving clarity and precision in product categorization. To develop an efficient purification method, several crystallizations were performed using a series of solvents of varying polarity (Table 1).

In the crystallization tests, methanol exhibited the worst behavior, not only in terms of the requested volume, which was the highest compared to all the other solvents, but also in terms of the yields of the purified product (Table 1, entry 3). The combination of dichloromethane as solvent and methanol as anti-solvent

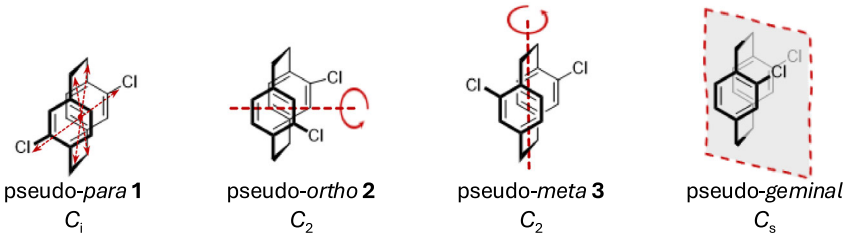

FIGURE 1 | Molecular structure and related symmetry group representations for the isomers of Galaxyl C.

TABLE 1 | Crystallization tests on Galaxyl C.

#	Solvent	Galaxyl C, g	Isomer 1, g	Solvent volume, mL	Solvent volume/ isomer 1, mL/g	Solvent volume/ Galaxyl C, mL/g	Isomer 1/ Galaxyl C, %
1	*n*-hexane	1.541	0.356	37	104	24	23
2	*n*-hexane	10.138	2.347	255	109	25	23
3	Methanol	1.570	0.321	150	465	95	20
4	Dichloromethane/ methanol	1.610	0.274	11	40	7	17
				15	55	9	
5	*n*-heptane	1.618	0.428	22	51	14	26

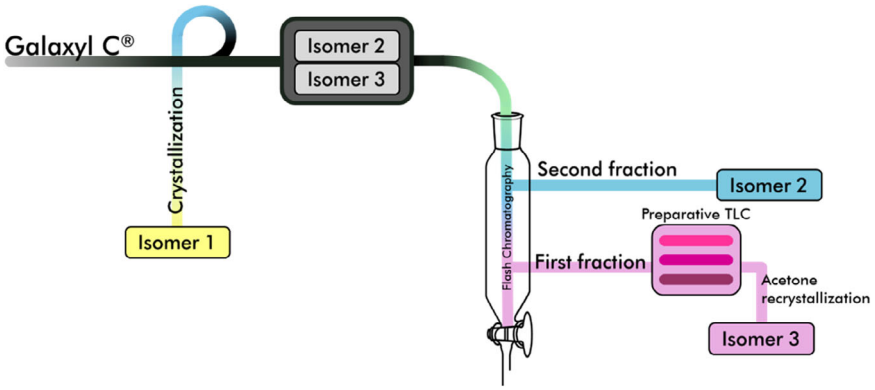

FIGURE 2 | Schematic procedure for isomers separation involving crystallization, chromatography, and preparative TLC.

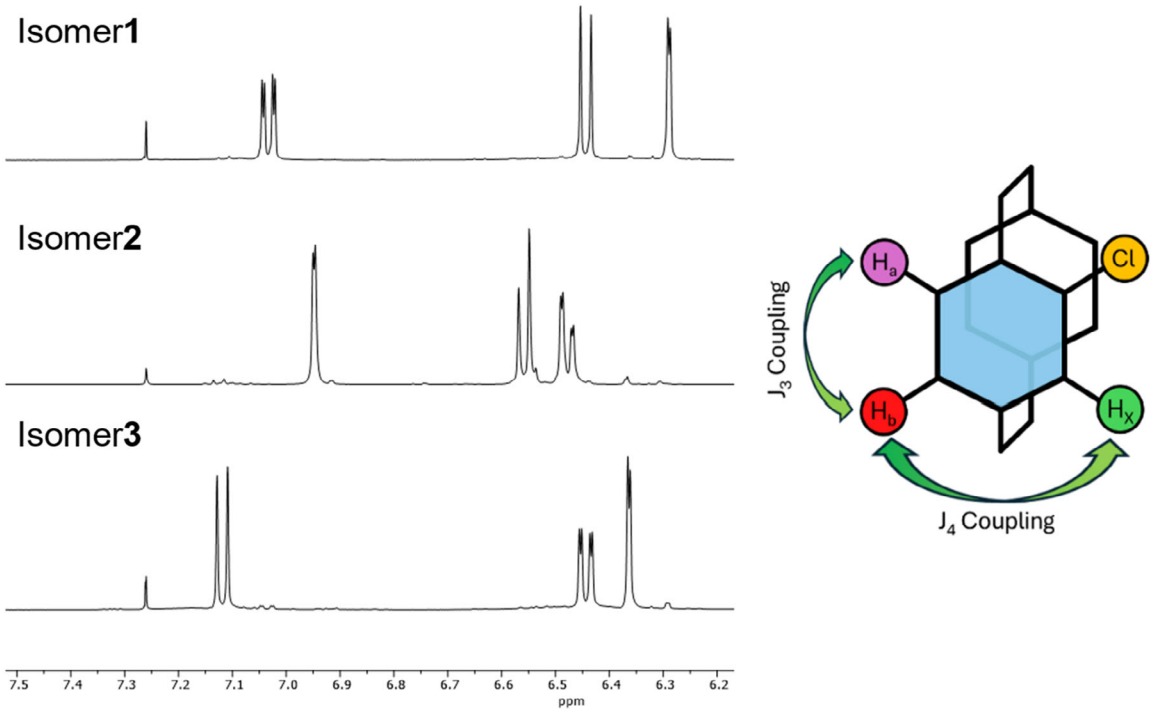

FIGURE 3 | Aromatic region of the ^{1}H NMR spectra in chloroform-*d* of the three different isolated isomers (left) and graphical representation of an ABX aromatic coupling system (right).

significantly reduced the volume of methanol required (Table 1, entry 4). However, this combination was not further investigated due to concerns regarding the hazards associated with the use of dichloromethane. Crystallization with *n*-hexane was effective and proved viable for scale-up (Table 1, entries 1–2). Then *n*-heptane was considered as a solvent with a similar polarity to *n*-hexane, reduced volatility, better hazard profile, and a higher boiling point capable of furnishing more concentrated supersaturated hot solutions of the mixtures. Crystallization with *n*-heptane required the lowest volume of solvent per gram of Galaxyl C and yielded the best percentage of pure isomer **1** (Table 1, entry 5). Overall, *n*-heptane was considered the best and safest option for isolating isomer **1** from the mixture of Galaxyl C.

After crystallization, the composition of the mother liquor was further purified by flash chromatography, obtaining two main fractions (Figure 2). ^{1}H NMR analysis of the second fraction showed the presence of a pure compound different from **1** (isomer **2**). The first fraction containing a mixture of products was further purified by preparative thin-layer chromatography (TLC), followed by crystallization from hot acetone to remove the remaining traces of isomer **2**. The acetone mother liquor was concentrated to dryness, showing the presence of a pure compound (corresponding to isomer **3**).

^{1}H NMR analysis of the three isolated isomeric compounds revealed distinct sets of ABX aromatic resonances (Figure 3).

2.2 | Structure Determination of Isomers

The four possible isomers of Cl_2-PCP can be classified according to their point group symmetry. The pseudo-*para* isomer is defined as C_i; thus, the only geometrical operation admitted, different from identity, is a punctual inversion. Both the pseudo-*ortho* and pseudo-*meta* isomers are defined as C_2, due to the presence of a 180° rotation axis. The last isomer, the

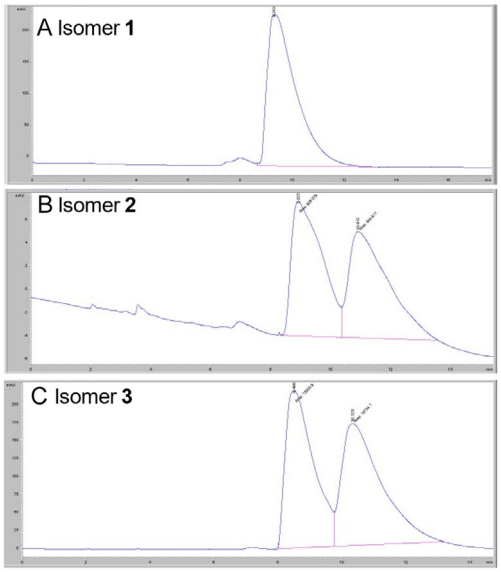

FIGURE 4 | Chromatograms of isomer **1** (A, above), isomer **2** (B, middle), and isomer **3** (C, below). Column: Cellulose-4, eluent: *n*-hexane, flow: 1.5 mL/min, λ of detector: 260 nm, injection volume: 75 µL, concentration: 0.1 mM.

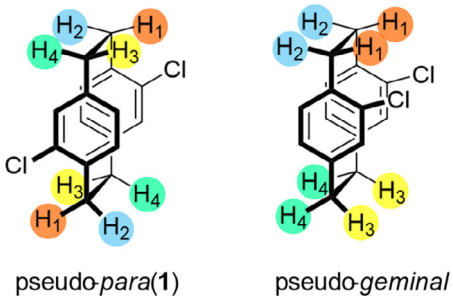

FIGURE 5 | Pseudo-*para* isomer **1** and pseudo-*geminal* isomer with aliphatic protons highlighted.

pseudo-*geminal*, is characterized by a planar symmetry, which confers to it the descriptor C_s (Figure 1).

In consideration of the different symmetry properties of the four isomers, the pseudo-*para* derivative, which is characterized by an inversion point, and the pseudo-*geminal* isomer, which contains a plane of symmetry in the molecule, are therefore achiral compounds. Conversely, the pseudo-*ortho* and pseudo-*meta* isomers are chiral. For this reason, isomers **1**, **2**, and **3** were subjected to chiral HPLC analysis (Figure 4). The chromatogram of isomers **2** and **3** showed two peaks, whereas isomer **1** consistently showed only one peak, regardless of the large series of chiral columns and experimental conditions tested; this clearly confirms that isomer **1** is achiral.

Since **1** was confirmed to be achiral, its structure could only correspond to isomers pseudo-*para* or pseudo-*geminal*. The existing literature concerning the NMR characterization of dichlorinated paracyclophane compounds is notably sparse. Consequently, we undertook an in-depth 1D and 2D NMR investigation and characterization of each isomer. In particular, for the pseudo-*para* isomer, the four bridging H atoms are all chemically inequivalent, resulting in four distinct chemical shifts. Each H atom shows different coupling constants with the other three H, leading to a complex ABCD spin system, where each H shows a multiplicity corresponding to a *ddd*. Conversely, for the pseudo-*geminal* isomer its C_s symmetry leads to four aliphatic protons divided into two sets, H_1 and H_2, with the same chemical environment but a different magnetic environment, corresponding to an AA′BB′ and CC′DD′ spin system showing two resonances each as a *dd* (Figure 5).

The ^{1}H NMR of **1** reported in Figure 6 shows clearly the presence of four sets of *ddd* signals for bridging aliphatic protons. This information agrees with the assignment of **1** to the pseudo-*para* structure.

To confirm this hypothesis, other NMR experiments were performed. The COZY coupling between protons H_1, H_2, H_3, and H_4 is possible only for the pseudo-*para* and -*ortho* isomers, in which these protons are less than four covalent bonds apart.

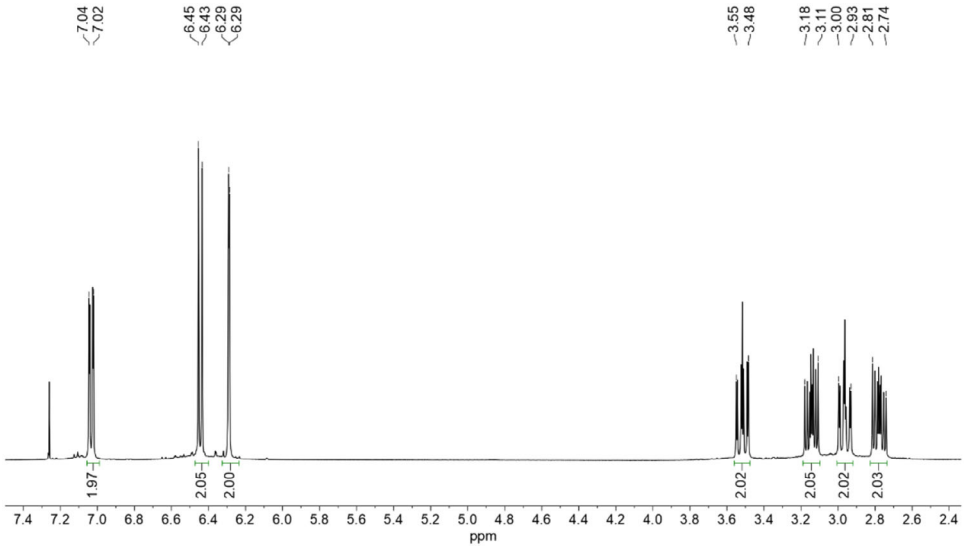

FIGURE 6 | ^{1}H NMR spectrum of isomer **1** in chloroform-*d* corresponding to the pseudo-*para* isomer.

In the case of the pseudo-*geminal* and *meta* isomers, the COSY interaction is not possible because of the larger distance that separates the nuclei. Conversely, NOESY interactions are possible only in the pseudo-*para* and -*ortho* isomers because of the proximity between aliphatic protons; such interactions in the pseudo-*geminal* and -*meta* isomers are too weak to be visible. Both COSY and NOESY spectra of **1** show correlations between all four aliphatic resonances (Figure 7B,C) further supporting the structural assignment of compound **1** as the pseudo-*para* isomer (further 2D spectra interpretations in the Supporting Information).

With similar 2D NMR analyses, the structures of isomers **2** and **3** were assigned to the corresponding pseudo-*ortho* and pseudo-*meta* derivatives, respectively (see Supporting Information). After this extensive NMR characterization, it was possible to ascertain the composition of Galaxyl C, with the pseudo-*meta* **3** being the most abundant isomer corresponding to 46%, followed by pseudo-*ortho* **2** at 29% and pseudo-*para* **1** at 25%. The absence of the pseudo-*geminal* isomer is likely to be due to the steric hindrance existing between two neighboring chlorine atoms (Figure 8).

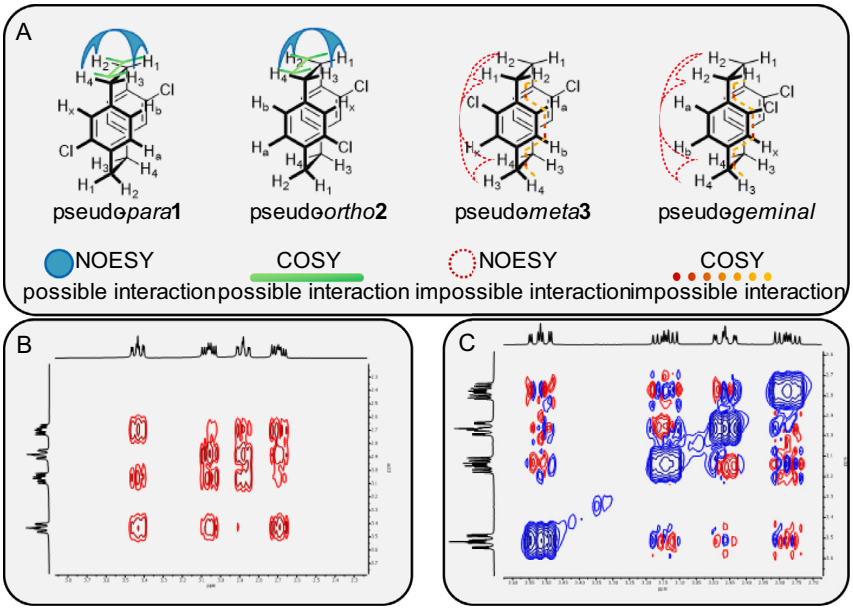

FIGURE 7 | (A) Expected and unexpected COSY/NOESY interactions for the four possible isomers; (B) aliphatic portion of the COZY spectrum of isomer **1**; and (C) aliphatic portion of the NOESY spectrum of isomer **1**.

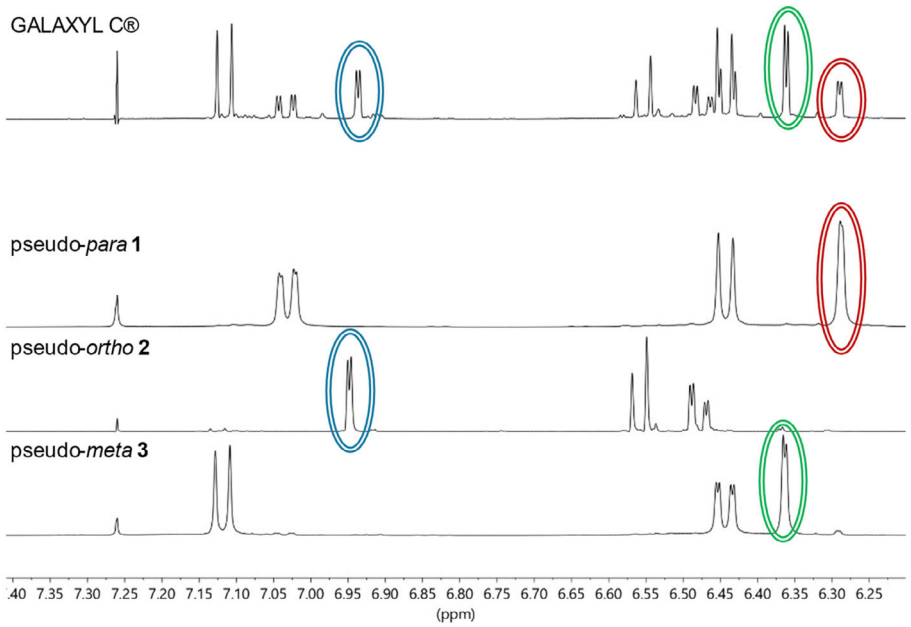

FIGURE 8 | Stacked ^{1}H NMR spectra in chloroform-*d* of Galaxyl C (above), pseudo-*para* **1**, pseudo-*ortho* **2**, and pseudo-*meta* **3** isomers. Protons H_X attributed to the three isomers are highlighted in different colors.

2.3 | Reaction of Pseudo-*para* 1 with *n*-Butyllithium

Isomer **1** was selected as a candidate for testing the reaction with *n*-butyllithium (BuLi) due to the ease of its purification, which gave rapid access to large amounts of material, free from protic impurities. Furthermore, the higher distance between the chlorine atoms in the molecular structure ensures the absence of reciprocal interferences on the reactivity. The first test was performed in diethyl ether (Et_2O), where a large excess of BuLi was added at −78°C, and then the mixture was allowed to warm to room temperature. The reaction was followed by GC–MS, showing a rather slow conversion of the starting material **1** with complete conversion in more than 90 h. The reaction afforded a crude containing a complex mixture of products with less than 40% relative area of the desired product **7**. In contrast, the remaining products were characterized by different combinations of butyl-dechlorination and hydro-dechlorination levels, as evidenced by GC–MS (Figures 9 and S13).

The single peaks observed in GC–MS for **7** exclude the hypothesis of a benzyne mechanism [48], because the latter intermediate allows the introduction of the butyl moiety either on the carbon bearing the chlorine atom or on the adjacent carbon bearing the hydrogen, leading to the 1:1 statistical formation of two constitutional isomers (pseudo-*para* and pseudo-*meta*). Alternatively, the alkylation mechanism, consisting of a first metal-halogen exchange step [49, 50] followed by a supposed substitution step that converts the halogen derivative into the alkylated species (Scheme 1A), should lead as observed to the formation of a single species with no isomeric forms for each product observed. The hydro-de-halogenation can be explained by a first metal-halogen exchange followed by deprotonation in the alpha position of 1-chlorobutane, yielding 1-butene as a coproduct (Scheme 1B).

Given these unsatisfactory initial results, a systematic optimization study was undertaken to favor the formation of the target dialkylated product **7**. The presence of by-products significantly complicated the purification of **7**, hindering both crystallization and chromatographic separation (for a detailed account of these experiments, see the Supporting Information).

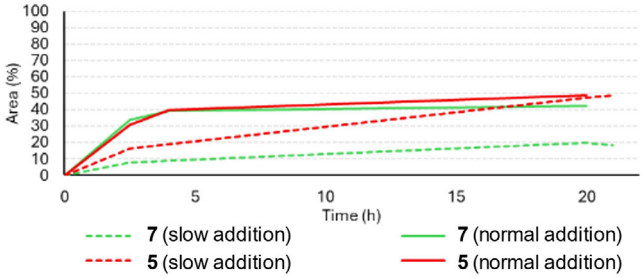

FIGURE 10 | Comparison of the product profile for slow and normal addition of BuLi.

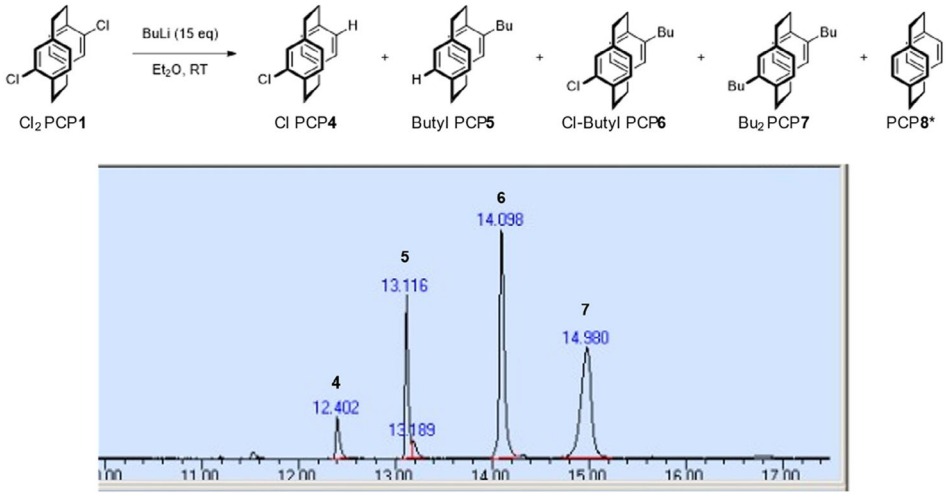

FIGURE 9 | Reaction scheme for the alkylation of pseudo-*para* isomer **1** with BuLi (top), and EI-MS chromatogram of the reaction mixture showing product composition (bottom). *Product **8** not found in the product mixture.

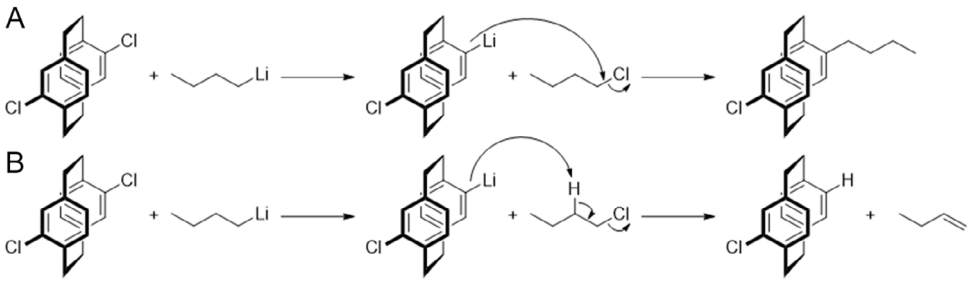

SCHEME 1 | (A) Proposed mechanism for the alkylation reaction and (B) proposed mechanism for the hydro-de-halogenation reaction.

The sluggish conversion observed was counterintuitive given the high reactivity of BuLi, suggesting potential degradation pathways. To investigate this, 6 equivalents of BuLi were added in three separate 2-equivalent aliquots (at $t = 0$, 5, and 22 h). Notably, this stepwise addition failed to accelerate the reaction; instead, it promoted the formation of a higher amount of by-product **5**, thereby lowering the percentage area of the desired dialkylated product **7** to less than 20%.

It is known that the presence of a chelating agent, such as *N*,*N*,*N*,*N*-tetramethyl ethylenediamine (TMEDA), interacting efficiently with lithium [51], can separate it from the carbon fragment, thus conferring a stronger reactivity to BuLi [52]. When BuLi was added to a mixture of **1** and TMEDA in diethyl ether, the starting material was consumed in less than 3 h. The relative amount of dialkylated **7** obtained was the same as in the reaction without TMEDA, but with a marked reduction in reaction time. Under such experimental conditions, another by-product was observed for the first time, corresponding to the unsubstituted [2.2]paracyclophane **8** obtained by the double hydro-de-chlorination.

Given the enhanced reactivity observed with TMEDA, we further investigated the effect of slow BuLi addition in combination with this chelating agent. When BuLi was introduced *via* syringe pump over 3 h, starting material **1** was completely consumed within 5.5 h of the start of addition. However, the yield of the desired product **7** remained below 20% (GC percentage area). Notably, this slow addition protocol increased selectivity

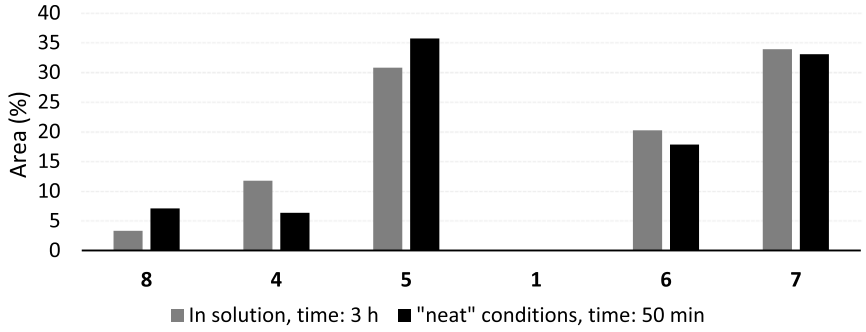

FIGURE 11 | Comparison of reaction outcome for reaction performed in solution and under "neat" conditions.

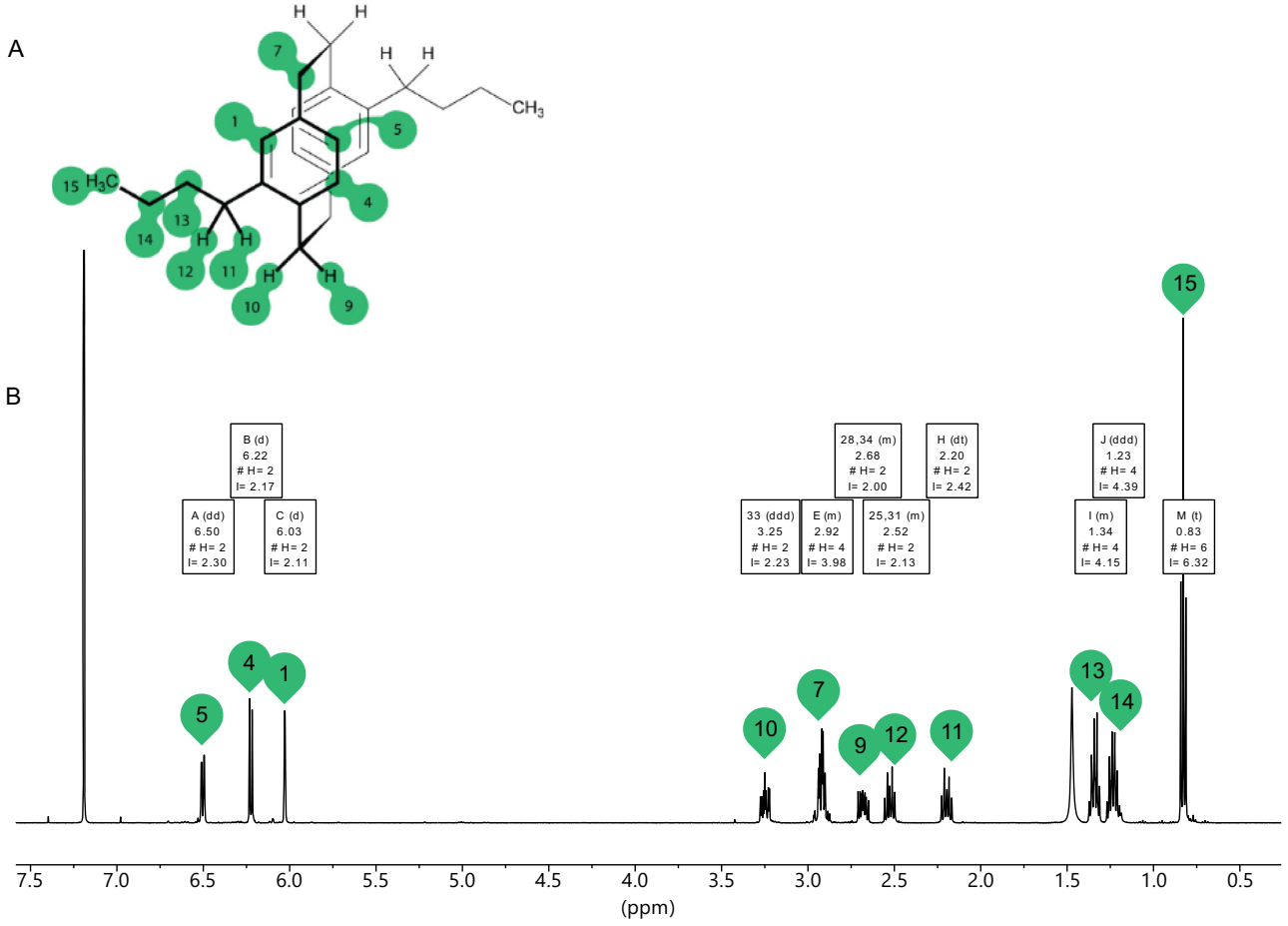

FIGURE 12 | Structure of **7** with proton labeled (A, upper) and ^{1}H NMR spectrum of isolated **7** (B, lower) in chloroform-*d*.

toward the monoalkylated-dehalogenated product **5** compared to the standard single shot addition (Figure 10).

To evaluate the feasibility of a solvent-free process, we investigated the elimination of diethyl ether as a bulk solvent. Given its essential coordinating properties, diethyl ether was instead employed in a stoichiometric ratio relative to BuLi, with the *n*-hexane from the commercial BuLi solution serving as the primary reaction medium. This modification significantly accelerated the formation of the target dialkylated product **7**. Remarkably, this approach maintained the product distribution observed in pure diethyl ether while achieving a three-fold increase in the reaction rate (Figure 11).

The rate acceleration under 'neat' conditions observed could be ascribed to the great exothermicity of the reaction during BuLi addition directly to **1**. To investigate the effect of temperature, an experiment was conducted by adding BuLi at −78°C and then maintaining the reaction at 0°C for 3 h. Under these conditions, a more selective formation of the monoalkylated product **5** was observed. Indeed, the relative ratio between the desired dialkylated product **7** and the monoalkylated derivative **5** was approximately halved, changing from a **7**/**5** ratio of 1.18 when the temperature was maintained at 25°C to 0.60 when the temperature was lowered to 0°C.

After this extensive study, the 'neat' conditions were discarded. The most effective conditions for the alkylation of **1** were identified using *n*-heptane as the solvent and BuLi in a *n*-heptane solution, facilitating the attainment of a reaction temperature of 98°C. Six equivalents of BuLi were introduced as a single, rapid shot into a solution containing **1**, together with six equivalents of TMEDA. Under these conditions, reagent **1** was consumed within 1 h, and the purification sequence consisted of an initial filtration through a silica pad, followed by preparative thin-layer chromatography. This optimized protocol afforded the pure target compound **7** in 22% overall yield. The full characterization of the product was performed using NMR spectroscopy (see Supporting Information).

The ^{1}H NMR spectrum of **7** provided crucial insights into its structural features. The benzylic methylene protons of the butyl chains exhibited two distinct signals, centred at 2.20 and 2.52 ppm, respectively. This observation is consistent with the inequivalent diastereotopic nature of the protons, resulting in distinct spectroscopic environments and separate resonances in the ^{1}H NMR spectrum (Figure 12). This characteristic splitting provided strong evidence for the precise connectivity and stereochemical arrangement of the butyl substituents in **7**.

3 | Conclusions

In conclusion, an effective procedure for the separation of Cl_2-PCP isomers was reported, successfully isolating the pseudo-*para* isomer from a commercial mixture and confirming the structure of the isomers by 1D and 2D NMR. An analysis of the composition of Galaxyl C was reported, showing the relative amounts of the different isomers (25% isomer **1**, 29% isomer **2**, and 46% isomer **3**), as well as the absence of the pseudo-*geminal* isomer. The more accessible pure isomer **1** was subjected to alkylation with BuLi, leading to a transition-metal-free protocol. Through extensive optimization, it was found that reaction rate and selectivity could be significantly enhanced by adding TMEDA, using *n*-heptane as the solvent, and increasing the reaction temperature to 98°C. After optimization, the percentage area of **7** (calculated *via* GC integration) was increased from 20% to 70%. The final optimized conditions yielded the desired dialkylated product **7** in an isolated yield of 22% after purification. This work not only offers a more efficient and sustainable synthetic method for the functionalization of Cl_2-PCP but also paves the way for future optimizations and the exploration of this new reactivity with other halogenated aromatic compounds.

Acknowledgments

The authors acknowledge Dr. Giuseppe Borsato and Dr. Matteo Bertoldini for GC-MS analyses and Galentis s.r.l. for providing samples of Galaxyl. A.S and F.F are grateful to Università Ca' Foscari for support.

Open access publishing facilitated by Universita Ca' Foscari, as part of the Wiley - CRUI-CARE agreement.

Funding

The authors have nothing to report.

Conflicts of Interest

The authors declare no conflicts of interest.

Data Availability Statement

The data that support the findings of this study are available from the corresponding author upon reasonable request.

References

1. H. Tappert and S. Bräse, "[2.2]Paracyclophane Materials—Status and Perspectives," *Macromolecular Rapid Communications* 46 (2025): 2500145.

2. C. Wang, H. Zhang, L. Chen, Z. Zhang, Y. Feng, and X. Cui, "Functionalization and Applications of [2.2] Paracyclophanes (PCPs)," *SynOpen* 9 (2025): 302.

3. D. S. Seferos, S. A. Trammell, G. C. Bazan, and J. G. Kushmeric, "Probing π-Coupling in Molecular Junctions," *Proceedings of the National Academy of Sciences of the United States of America* 102 (2005): 8821.

4. S. E. Gibson and J. D. Knight, "[2.2]Paracyclophane Derivatives in Asymmetric Catalysis," *Organic & Biomolecular Chemistry* 1 (2003): 1256.

5. S. H. Gilbert, S. Tin, J. A. Fuentes, T. Fanjul, and M. L. Clarke, "Rhodium Catalysts Derived from a Fluorinated Phanephos Ligand Are Highly Active Catalysts for Direct Asymmetric Reductive Amination of Secondary Amines," *Tetrahedron* 80 (2021): 131863.

6. S. V. Kumar and P. J. Guiry, "Enantioselective Organozinc Addition to Aldehydes Using Planar Chiral [2.2]Paracyclophane-Imidazoline N,O-Ligands," *Chemistry – A European Journal* 30 (2024): e202403345.

7. S. Kitagaki, T. Nakayoshi, S. Masunaka, et al., "Highly Regio- and Stereoselective (3 + 2) Annulation Reaction of Allenoates with 3-Methyleneindolin-2-Ones Catalyzed by a Planar Chiral [2.2]paracyclophane-Based Bifunctional Phosphine–Phenol Catalyst," *Organic & Biomolecular Chemistry* 22 (2024): 7817.

8. C. Zippel, Z. Hassan, M. Nieger, and S. Bräse, "Design and Synthesis of a [2.2]Paracyclophane-Based Planar Chiral Dirhodium Catalyst and Its Applications in Cyclopropanation Reaction of Vinylarenes with α-Methyl-α-Diazo Esters," *Advanced Synthesis & Catalysis* 362 (2020): 3431.

9. L. Vaghi, R. Cirilli, M. Pierini, S. Rizzo, G. Terraneo, and T. Benincor, "PHANE-TetraPHOS, the First D_2 Symmetric Chiral Tetraphosphane. Synthesis, Metal Complexation, and Application in Homogeneous Stereoselective Hydrogenation," *European Journal of Organic Chemistry* 2021 (2021): 2367.

10. S. C. Huo, R. R. Indurmuddam, B. C. Hong, C. F. Lua, and S. Y. Chien, "The Hamburger-Shape Photocatalyst: Thioxanthone-Based Chiral [2.2] Paracyclophane for Enantioselective Visible-Light Photocatalysis of 3-Methylquinoxalin-2(1*H*)-One and Styrenes," *Organic & Biomolecular Chemistry* 21 (2023): 9330.

11. Z. H. Zhu, Y. X. Ding, and Y. G. Zhou, "Biomimetic Reduction of Imines and Heteroaromatics with Chiral and Regenerable [2.2] Paracyclophane-Based NAD(P)H Model CYNAM," *Tetrahedron* 83 (2021): 131968.

12. J. Brom, A. Maruani, S. Turcaud, et al., "[2.2]Paracyclophane-Based Coumarins: Effective Organo-Photocatalysts for Light-Induced Desulfonylation Processes," *Organic & Biomolecular Chemistry* 22 (2024): 59.

13. Y.-Q. Bai, X.-W. Wang, B. Wu, et al., "Design and Synthesis of Planar-Chiral Oxazole–Pyridine *N*,*N*-Ligands: Application in Palladium-Catalyzed Asymmetric Acetoxylative Cyclization," *ACS Catalysis* 13 (2023): 9829.

14. J. Wang, Q.-X. Xie, X. Li, C.-B. Yu, and Y.-G. Zhou, "Synthesis of Planar-Chiral [2.2]Paracyclophane-Based Oxazole-Pyrimidine Ligands and Application in Nickel-Catalyzed 1,2-Reduction of α,β-Unsaturated Ketones," *Chinese Journal of Chemistry* 42 (2024): 705.

15. M. Gon, Y. Morisaki, and Y. Chujo, "Optically Active Phenylethene Dimers Based on Planar Chiral Tetrasubstituted [2.2]Paracyclophane," *Chemistry – A European Journal* 23 (2017): 6323.

16. X. Li, Y. Xie, and Z. Li, "The Progress of Circularly Polarized Luminescence in Chiral Purely Organic Materials," *Advanced Photonics Research* 2 (2021): 2000136.

17. D. W. Zhang, J. M. Teng, Y. F. Wang, X. N. Han, M. Li, and C. F. Chen, "D–π*–A Type Planar Chiral TADF Materials for Efficient Circularly Polarized Electroluminescence," *Materials Horizons* 8 (2021): 3417.

18. K. Kikuchi, J. Nakamura, Y. Nagata, et al., "Control of Circularly Polarized Luminescence by Orientation of Stacked π-Electron Systems," *Chemistry – An Asian Journal* 14 (2019): 1681.

19. Y. Sasai, R. Inoue, and Y. Morisaki, "Synthesis and Chiroptical Properties of †- and ‡-Shaped Molecules Based on Planar Chiral [2.2] Paracyclophane," *Bulletin of the Chemical Society of Japan* 93 (2020): 1193.

20. G. Namba, Y. Mimura, Y. Imai, R. Inoue, and Y. Morisaki, "Control of Axial Chirality by Planar Chirality Based on Optically Active [2.2] Paracyclophane," *Chemistry – A European Journal* 26 (2020): 14871.

21. A. K. Gupta, Z. Zhang, E. Spuling, et al., "Electron-Withdrawing Group Modified Carbazolophane Donors for Deep Blue Thermally Activated Delayed Fluorescence OLEDs," *Materials Advances* 2 (2021): 6684.

22. P. Li, W. Li, X. Wang, et al., "High-Performance Circular Polarization Multiple-Resonance TADF Molecules with Enhanced Long-Range Charge Transfer Based on Chiral Paracyclophane," *Journal of Physical Chemistry Letters* 16 (2025): 340.

23. Z. Hassan, "Molecular Insights Into [2.2]Paracyclophane-Based Functional Materials: Chemical Aspects Behind Functions," *Advanced Functional Materials* 34 (2024): 2311828.

24. H. Kim, B. Noh, C. B. Lee, et al., "Nanoscopic Parylene Layer: Enhancing Perovskite Solar Cells Through Parylene-D Passivation," *Small Methods* 10 (2025): 2500395.

25. C. N. Tsai, C. Y. Lee, H. Y. Chen, and B. C. Hsieh, "Parylene Double-Layer Coated Screen-Printed Carbon Electrode for Label-Free and Reagentless Capacitive Aptasensing of Gliadin," *ACS Sensors* 9 (2024): 3689.

26. T. H. Kim, Z. Song, J. Jung, et al., "Functionalized Parylene Films for Enhancement of Antibody Production by Hybridoma Cells," *ACS Applied Bio Materials* 6 (2023): 3726.

27. S. C. Jang, G. Lee, I. Park, et al., "Tunable Dielectric Properties of a Parylene Dielectric Layer Through Surface-Modulation by Click Chemistry," *Journal of Materials Chemistry C: Materials for Optical and Electronic Devices* 13 (2025): 6614.

28. E. Afshari, S. Houri, R. Verplancke, et al., "Biocompatible and Hermetic Encapsulation of PMUTs: Effects of Parylene F-VT4 and ALD Stacks on Membrane Vibration and Acoustic Performance," *Sensors* 25 (2025): 4074.

29. M. Plank, A. Berardi, A. Welle, et al., "Photo-Arbuzov Reactions as a Broadly Applicable Surface Modification Strategy," *Advanced Functional Materials* 34 (2024): 2403408.

30. J. Chen, W. Duan, Z. Chen, M. Ma, C. Song, and Y. Ma, "[2.2] Paracyclophane-Based Carbene–Copper Catalyst Tuned by Transannular Electronic Effects for Asymmetric Boration," *RSC Advances* 6 (2016): 75144.

31. J. P. Seymour, Y. M. Elkasabi, H. Y. Chen, J. Lahann, and D. R. Kipke, "The Insulation Performance of Reactive Parylene Films in Implantable Electronic Devices," *Biomaterials* 30 (2009): 6158.

32. J. LahannH. Höcker, and R. Langer, "Synthesis of Amino[2.2]paracyclophanes-Beneficial Monomers for Bioactive Coating of Medical Implant Materials," *Angewandte Chemie, International Edition* 40 (2001): 726.

33. P. Hanefeld, S. Agarwal, R. Kumar, and A. Greiner, "In Vitro Study of Dexamethasone Release From Poly(*p*-xylylene) Films," *Macromolecular Chemistry and Physics* 211 (2010): 265.

34. N. Iguchi, H. Kasanuki, N. Matsuda, M. Shoda, S. Ohnishi, and S. P. Hosoda, "Contact Sensitivity to Polychloroparaxylene-Coated Cardiac Pacemaker," *Pacing and Clinical Electrophysiology* 20 (1997): 372.

35. Verified Market Research, "*Global Parylene Market Size by Type of Parylene, by Application, by End-Use Industries, By Geographic Scope and Forecast*," (2024), Accessed October16, 2025, https://www.verifiedmarketresearch.com/product/parylene-market/.

36. A. Greiner, S. Mang, O. Schäfer, and P. Simon, "Poly(*P*-xylylene)s: Synthesis, Polymer Analogous Reactions, and Perspectives on Structure–Property Relationships," *Acta Polymerica* 48 (1997): 1.

37. J. B. Fortin and T. M. Lu, Film Properties in *Chemical Vapor Deposition Polymerization: The Growth and Properties of Parylene Thin Films* (Kluwer, 2003).

38. B. J. Kim and E. Meng, "Micromachining of Parylene C for bioMEMS: Micromachining of Parylene C for BioMEMS," *Polymers for Advanced Technologies* 27 (2016): 564.

39. A. Baldwin and E. Meng, "A Kirigami-Based Parylene C Stretch Sensor," *MEMS* 227 (2017).

40. O. Schäfer, F. Brink-Spalink, B. Smarsly, et al., "Synthesis and Properties of ω-Phenylalkyl-Substituted Poly(*p*-xylylene)s Prepared by Base-Induced 1,6-Dehydrohalogenation," *Macromolecular Chemistry and Physics* 200 (1999): 1942.

41. M. Ishaque, R. Wombacher, J. H. Wendorff, and A. Greiner, "Synthesis and Structure-Property Relationships of Novel Poly (*p*-xylylene)s with Aromatic Substituents," *e-Polymers* 5 (2001): 1.

42. M. Ishaque, A. Greiner, and S. Agarwal, "Synthesis and Properties of Novel Poly (*p*-xylylene)s with Aliphatic Substituents," *e-Polymers* 2 (2002): 1.

43. W. F. Gorham, "Alkylated Di-*p*-Xylylenes," Union Carbide Corp. U.S. Patent 3 117 168 (1964).

44. Y. L. G. Yeh and F. William, "Preparation and Reactions of Some [2.2] Paracyclophane Derivatives," *Journal of Organic Chemistry* 34 (1969): 2366.

45. L. Ying and Y. Yeh, "Process for the Preparation of Alkylated Di-*p*-Xylylenes," Union Carbide Corp. U.S. Patent 3 349 142 (1967).

46. A. K. Bier, M. Bognitzki, J. Mogk, and A. Greiner, "Synthesis, Structure, and Properties of Alkyl-Substituted PPXs by Chemical Vapor Deposition for Stent Coatings," *Macromolecules* 45 (2012): 1151.

47. R. P. O. David, "Syntheses and Applications of Disubstituted [2.2] Paracyclophanes," *Tetrahedron* 68 (2012): 8977.

48. X. Zhang, Y. Zhou, Z.-X. Yu, C.-H. Tung, and Z. Xu, "Strained Dehydro-[2,2]-Paracyclophane Enabled Planar Chirality Construction and [2.2]Paracyclophane Functionalization," *Angewandte Chemie, International Edition* 64 (2025): e202420667.

49. H. Gilman, W. Langham, and F. W. Moore, "Some Interconversion Reactions of Organolithium Compounds," *Journal of the American Chemical Society* 62 (1940): 2327.

50. H. R. Rogers and J. Honk, "Preliminary Studies of the Mechanism of Metal-Halogen Exchange. The Kinetics of Reaction of *n*-Butyllithium with Substituted Bromobenzenes in Hexane Solution," *Journal of the American Chemical Society* 104 (1982): 522.

51. D. Hoffmann and D. B. Collum, "Binding of Diamines to *n*-Butyllithium Dimers: Relative Solvation Energies and Evidence of Correlated Solvation," *Journal of the American Chemical Society* 120 (1998): 5810.

52. C. G. Screttas and J. F. Eastham, "Alkyllithium-Amine Crystalline Complexes," *Journal of the American Chemical Society* 87 (1965): 3276.

Supporting Information

Additional supporting information can be found online in the Supporting Information section. Elucidation of the molecular structures of **1**, **2** and **3**, experimental details, and characterization spectra of **1-3** and **7** are available in the Supporting Information. **Supporting Fig. S1:** Aliphatic portion of the HSQC spectrum of isomer **1** with colour legend for aliphatic protons. **Supporting Fig. S2:** Aliphatic portion of the HMBC spectrum of isomer **1** with colour legend for the aliphatic protons. **Supporting Fig. S3:** NOESY interactions observed between aromatic and aliphatic protons in isomer **1** (a segment of the spectrum has been omitted for clarity). **Supporting Fig. S4:** ^{1}H NMR spectrum of pseudo-*ortho* isomer **2**. **Supporting Fig. S5:** Aliphatic portion of the HSQC spectrum of pseudo-*ortho* isomer **2**. **Supporting Fig. S6:** NOESY spectrum showing the correlation between aliphatic and aromatic protons of pseudo-*ortho* isomer **2**. **Supporting Fig. S7:** NOESY spectrum of pseudo-*ortho* isomer **2**. The interaction between protons H_a and H_b (red-purple circle) is highlighted. **Supporting Fig. S8:** ^{1}H NMR spectrum of pseudo-*meta* isomer **3**. **Supporting Fig. S9:** Aliphatic portion of the HSQC spectrum of pseudo-*meta* isomer **3**. **Supporting Fig. S10:** NOESY spectrum of pseudo-*meta* isomer **3**, showing the correlation between aliphatic and aromatic protons. **Supporting Fig. S11:** NOESY spectrum of pseudo-*meta* isomer **3**. The interaction between protons H_b and H_x (green-red circle) is highlighted. **Supporting Fig. S12:** Graphical representation of isomer pseudo-*meta* **3** (left) and pseudo-*geminal* **4** (right), in which are shown the possible and impossible NOESY interactions. **Supporting Fig. S13:** Structure of products (top), GC chromatogram (black box), mass spectra, and fragmentation pattern of **8** (red box), **4** (orange box), **5** (yellow box), **1** (blue box), **6** (purple box), and **7** (green box). Zoom of the isotopic cluster for **1** and **7**. **Supporting Fig. S14:** Product distribution over time for the reaction of **1** with BuLi. The percentage area was calculated as the relative area of the product peaks over the total area. **Supporting Fig. S15:** Product distribution over time for the reaction of **1** with BuLi added in three steps. The percentage area was calculated as the relative area of the product peaks over the total area. **Supporting Fig. S16:** Product distribution over time for the reaction of **1** with BuLi in the presence of TMEDA. The percentage area was calculated as the relative area of the product peaks over the total area. **Supporting Fig. S17:** Product distribution over time for the reaction of **1** in the presence of TMEDA and slow addition of BuLi. The percentage area was calculated as the relative area of the product peaks over the total area. **Supporting Fig. S18:** ^{1}H NMR of **1** in chloroform-*d*. **Supporting Fig. S19:** ^{13}C NMR of **1** in chloroform-*d*. **Supporting Fig. S20:** COSY of **1** in chloroform-*d*. **Supporting Fig. S21:** HSQC of **1** in chloroform-*d*. **Supporting Fig. S22:** HMBC of **1** in chloroform-*d*. **Supporting Fig. S23:** NOESY of **1** in chloroform-*d*. **Supporting Fig. S24:** ^{1}H NMR of **2** in chloroform-*d*. **Supporting Fig. S25:** ^{13}C NMR of **2** in chloroform-*d*. **Supporting Fig. S26:** COSY of **2** in chloroform-*d*. **Supporting Fig. S27:** HSQC of **2** in chloroform-*d*. **Supporting Fig. S28:** HMBC of **2** in chloroform-*d*. **Supporting Fig. S29:** NOESY of **2** in chloroform-*d*. **Supporting Fig. S30:** ^{1}H NMR of **3** in chloroform-*d*. **Supporting Fig. S31:** ^{13}C NMR of **3** in chloroform-*d*. **Supporting Fig. S32:** COSY of **3** in chloroform-*d*. **Supporting Fig. S33:** HSQC of **3** in chloroform-*d*. **Supporting Fig. S34:** HMBC of **3** in chloroform-*d*. **Supporting Fig. S35:** NOESY of **3** in chloroform-*d*. **Supporting Fig. S36:** ^{1}H NMR of **7** in chloroform-*d*. **Supporting Fig. S37:** ^{13}C NMR of **7** in chloroform-*d*. **Supporting Fig. S38:** COSY of **7** in chloroform-*d*. **Supporting Fig. S39:** HSQC of **7** in chloroform-*d*. **Supporting Fig. S40:** HMBC of **7** in chloroform-*d*. **Supporting Fig. S41:** NOESY of **7** in chloroform-*d*. **Supporting Table S1:** GC-MS instrument specifications.